metals

MDPI

Article

Effects of Homogenization Heat Treatment on Mechanical Properties of Inconel 718 Sandwich Structures Manufactured by Selective Laser Melting

Sebastian Marian Zaharia [1,*], Lucia Antoneta Chicoș [1], Camil Lancea [1] and Mihai Alin Pop [2]

[1] Department of Manufacturing Engineering, Transilvania University of Brasov, 500036 Brasov, Romania; l.chicos@unitbv.ro (L.A.C.); camil@unitbv.ro (C.L.)
[2] Department of Materials Science, Transilvania University of Brasov, 500036 Brasov, Romania; mihai.pop@unitbv.ro
* Correspondence: zaharia_sebastian@unitbv.ro; Tel.: +40-749045767

Received: 31 March 2020; Accepted: 15 May 2020; Published: 16 May 2020

Abstract: In this study, lightweight sandwich structures with honeycomb cores are proposed and their mechanical properties are investigated through experiments and FEA (finite element analysis) simulation. Sandwich structures were fabricated out of Inconel 718 using selective laser melting technique with two different topologies—sandwich structures with perforated skin (SSPS) and sandwich structures with perforated core (SSPC). In addition, the effect of the homogenization heat treatment on the mechanical properties of the sandwich samples subjected to compression and microhardness tests was analyzed. Results showed significant increases of mechanical performance before and after homogenization heat treatment of the Inconel 718 samples. Microstructure analysis was performed to compare the microstructures before and after homogenization heat treatment for Inconel 718 alloys manufactured by selective laser melting (SLM). The accuracy of experimental data were evaluated by modeling of sandwich samples in Ansys software at the end of this study.

Keywords: selective laser melting; Inconel 718 alloy; mechanical properties; homogenization heat treatment; sandwich structures

1. Introduction

Selective laser melting (SLM) technology is able to manufacture metal parts with complex geometries, which are difficult to obtain by conventional manufacturing methods. During the SLM process, the metal powder particles are selectively melted by a laser beam, after which they are cooled rapidly and solidified. After solidification, a new powder layer is deposited and exposed to the laser beam again, this process is repeated until the part is completely built [1,2].

The manufacturing of Inconel 718 (nickel-based superalloy) using SLM technology is an intensely researched and widespread field because many manufacturers of SLM equipment offer this type of metal powder. Due to excellent creep resistance, good oxidation, high corrosion temperature and good fatigue life, Inconel 718 alloy are widely used in the automotive, aerospace (turbine blades, rocket engines), nuclear (reactors) and petrochemical industries [3–5]. Conventional heat treatments comprise solid solution annealing or homogenization together with double aging treatments commonly used for wrought or cast of Inconel 718 alloy samples [6,7]. Post heat treatment processes are normally used for Inconel 718 SLM samples to improve the microstructure homogeneity [8–11], corrosions behavior [12], mechanical performances [1,13–16].

The repeated fast thermal heating and cooling cycles of parts manufactured by SLM technology also induced a high level of residual thermal stresses in the top parts. Therefore, the SLM samples need

post heat treatment to homogenize the microstructure and relieve the residual stresses, in order to achieve the desired microstructure and mechanical properties [13]. A series of comparative researches investigated the microstructure and mechanical properties [17,18], fatigue crack growth [19], of AM (Additive Manufacturing) Inconel 718 samples without heat treatment (as-fabricated) in comparison with treated samples. Some studies have focused on the influence of manufacturing parameters on mechanical properties, porosity and microstructure [20], on surface morphologies and phases [21], of Inconel 718 samples fabricated by SLM. Many authors have centered their work on determining the microhardness of Inconel 718 samples manufactured by SLM [22–26].

There are simulation works in the literature which investigated the SLM process through various finite element modeling techniques of AM Inconel 718. Luo et al. [27] has developed a new efficient and accurate FE model for predicting transient material thermal behavior during the SLM process in part-level. Andreotta et al. [28] studied and modeled efforts that neglect Marangoni flow by coupling computational fluid dynamics (CFD) with heat transfer physics to simulate all active physical phenomena within the melt pool. Mukherjee et al. [29] predicted and experimentally measured residual stress components for Inconel 718 builds made by SLM. Remano et al. [30] have utilized a finite element method model to investigate molten and solidified Inconel 718 during the laser-based additive manufacturing.

Lightweight sandwich structures are manufactured by adhering two thin but strong skins to lightweight and thick core. Light materials, e.g., honeycomb panels (balsa wood, aluminum alloys, titanium and copper alloys, nickel alloys, iron alloys, fiber glass, carbon fibers) and polyurethane foam are often chosen as the core; strong materials which have high stiffness, such as carbon fiber reinforced polymer (CFRP), glass fiber reinforced polymer (GFRP), aluminum alloys, are used as the skins [31]. The main advantages of a sandwich structure are high bending strength-to-weight, improved fatigue life, steadiness under compressive forces, good thermal and acoustic isolation properties and high stiffness-to-weight ratios. The sandwich structure has been widely used in shipbuilding, automotive and aerospace industries (airplane floors, leading and trailing edges in wings, fuselage components and helicopter rotor blades). The most widely used core is the hexagonal cell lattice, also known as the honeycomb.

Compressive load studies on mechanical performances have been conducted on 316 L stainless steel honeycomb cellular cores [32], prismatic cellular materials, specifically hexagonal honeycombs manufactured with four different AM processes [33], and hexagonal lattice parts made by polymer AM [34]. SLM technology allows the manufacture of strong and complex lightweight structures with geometry that is unachievable by conventional manufacturing methods, including complex lattice structures [35,36]. Lightweight lattice structures are topologically ordered, three dimensional open-celled structures designed of one or more repeating unit cells [35]. Recent studies have focused on the microstructure–topology effects on the quasi-static and dynamic behavior [37], but also on deformation mechanisms and post-yielding behavior of lattice structures manufactured by Inconel 718 [38].

SLM technology provides opportunities to design and manufacturing complex sandwich structure and cellular architecture. It can be concluded from above-mentioned literatures that there are no honeycomb core sandwich structures manufactured directly by SLM technology. These types of sandwich structures cannot be manufactured because metal powder would remain inside the honeycomb cells which cannot be removed and would consequently lead to a significant increase in the weight of the structures. The direct manufacture of honeycomb core sandwich structures by SLM technology can be done in two ways: the first one is to manufacture the skins and the honeycomb core separately and then bond them; the second one is to design the structures with holes in order to remove the metal powder. In this study, two types of honeycomb core sandwich structures were designed with holes, in the shell or in the core so as to remove the metallic powder easily. Moreover, a comparative analysis of the microstructure and the mechanical performances (compression, microhardness) between as-fabricated sandwich structures and the sandwich structures

subjected to the homogenization treatment was investigated in this study. The compression tests were validated by finite element analysis for the two sandwich structures (perforated core and perforated skin) manufactured by SLM technology.

2. Materials and Methods

2.1. Design of Sandwich Structures

The sandwich structures with honeycomb core were modeled in the SolidWorks software (SolidWorks 2019, Dassault Systems, Velizy-Villacoublay, France). The design of honeycomb core sandwich structures started from limitations regarding their manufacture by SLM technology. Thus, sandwich structures cannot be directly manufactured by SLM technology because the inside of the hexagonal honeycomb core would be filled with metallic powder. In order to eliminate this drawback, in this study it was decided to perforate the skin or the core of the sandwich structures to remove the metal powder. Thus, two identical types of sandwich structures were designed, for which 2 mm diameter holes were inserted in the skin (Figure 1a) or in the honeycomb core (Figure 1b). The specimens had the dimensions of 30 mm (length) × 30 mm (width) × 15 mm (thickness) and the thickness of the skin was 1 mm. In the current study, sandwich structures with hexagonal honeycombs (Figure 1c) were manufactured using SLM with wall thickness (t) 0.6 mm, with a cell size (D) of 8.98 mm and side length (a) 5.19 mm.

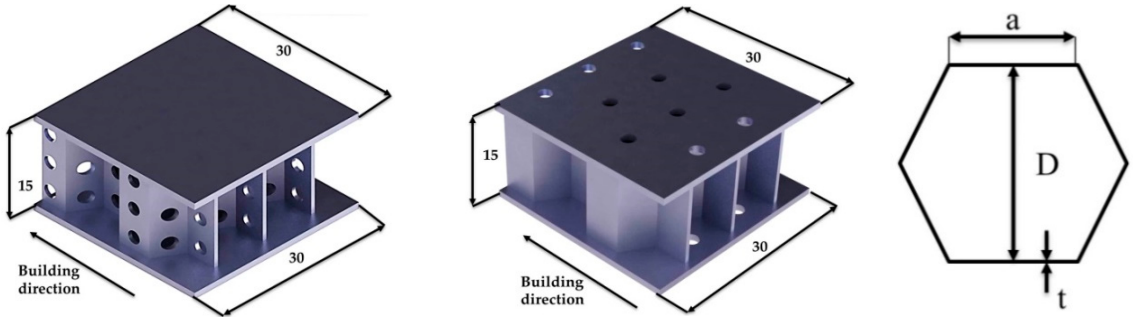

Figure 1. Three-dimensional models (mm): (**a**) sandwich structures with perforated core (SSPC); (**b**) sandwich structures with perforated skin (SSPS); (**c**) details of the hexagonal core.

2.2. SLM Fabrication of Samples

The samples were manufactured using a SLM 280HL (SLM Solution Group AG, Lübeck Germany) system equipped 2x400 W yttrium fiber lasers within a build chamber of 280 × 280 × 350 mm^3 [39]. The material of this study was gas atomized Inconel 718 alloy powder with spherical particles in the diameter range from 10 to 45 μm [40]. The manufacturing process of sandwich structures with honeycomb core was carried out at SLM Solutions Company from Luebeck, Germany. The chemical composition of this metal powder is listed in Table 1.

Table 1. Chemical composition in wt% of the Inconel 718 SLM GmbH (Lübeck, Germany) powders used in this study [41].

Ni	Cr	Ta + Nb	Mo	Ti	Al	Fe
50–55	17–21	4.75–5.50	2.80–3.30	0.65–1.15	0.20–0.80	
Cu	**C**	**Si, Mn**	**B**	**Co**	**P, S**	balance
0.30	0.08	0.35 each	0.006	1.00	0.015 each	

In the manufacturing process of all sandwich structures by SLM method the following parameters were used: laser power—200 W, scanning speed—900 mm/s, hatch distance—120 µm, layer thickness—30 µm, parts were manufactured in argon atmosphere. For this study, 20 sandwich structures made of Inconel 718 were manufactured (10 specimens with holes on the surface of the skin and 10 specimens with holes on the surface of the core). The measured sandwich structures were subsequently compared with the nominal dimension from the CAD file and the results (along the three axes) showed a geometric deviation of approximately 0.03 mm.

2.3. Heat Treatment of Samples

The sandwich structures manufactured by SLM technology were heat-treated with the following schedule in this study: homogenization treatment 1080 °C, 1.5 h/air cooling (AC) + solution treatment 980 °C, 1 h/air cooling + double aging 720 °C, 8 h/furnace cooling (FC) at 55 °C/h to 620 °C, 8 h/air cooling, according to industrial standard heat treatment for casting IN718 [42,43]. Figure 2 shows a graphical representation of the homogenization heat treatment schedule of the sandwich specimens. The optical images of Inconel 718 samples were taken with a metallographic microscope Nikon Eclipse MA 100 (Nikon Corp., Tokyo, Japan).

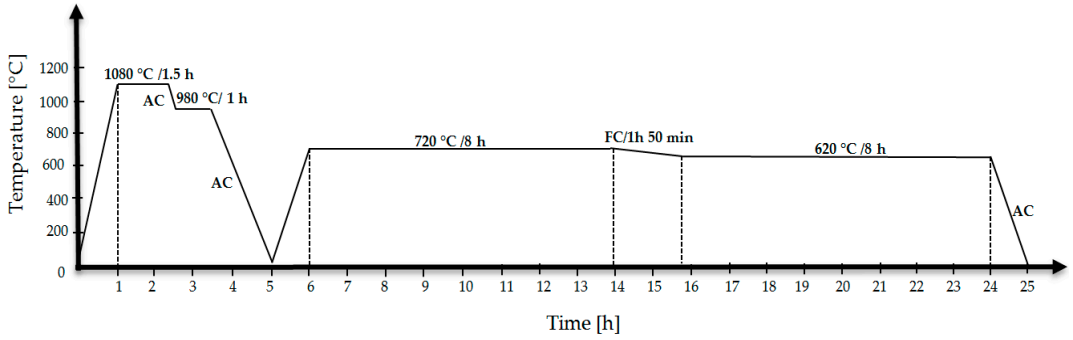

Figure 2. Schematic diagram of the homogenization heat treatment process.

2.4. Compression Test of Sandwich Structures

Twenty sandwich structures with honeycomb core made of Inconel 718 manufactured by SLM underwent the compression testing using a WDW-150S universal testing machine (Jinan Testing Equipment IE Corporation, Jinan, China). All compression tests were carried out under displacement control at a constant cross-head speed of 2 mm/min. The universal test machine was equipped with a displacement transducer on the drive screw that offers an accuracy of 0.01 mm. The dimensions of the sandwich structures compression tested in this study were manufactured, according to ASTM Standard C365 and MIL Standard 401.B. For the compression tests, the following sandwich specimen dimensions (according to MIL Standard 401.B) were introduced into the test machine program: 30 mm (length) × 30 mm (width) × 15 mm (height). The standardized calculation relationships of mechanical tests were entered by the manufacturer in the software of the equipment and the value of the compression strength and compression module was automatically generated in the test report.

2.5. Microhardness of Samples

For analysis of microhardness of the sandwich structures was, the samples were cut in vertical cross section—parallel to the building direction (Figure 3)—embedded in epoxy resin and then ground with sandpaper by gradual changing of the grain (600, 1200, 1500, 2000 and 2500) using a semi-automated grinding system (Phoenix Beta, Buehler, IL, USA).

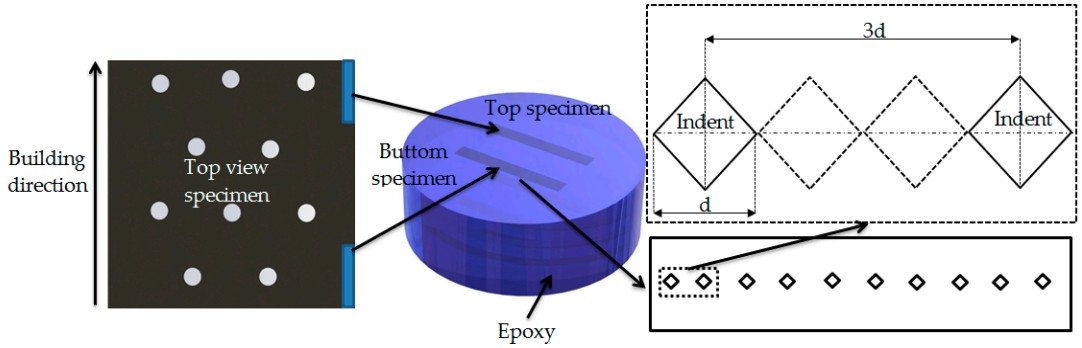

Figure 3. A schematic view of the location on which microhardness testing was performed on the sandwich specimen.

Microhardness was measured 10 times for each specimen using the microhardness tester (Future-Tech FM-700, Future-Tech Corp, Tokyo, Japan) at a 100 gf. load and a loading time of 15 s. The spacing between indents should be at least 3 times the d length for the Vickers test.

The statistical analysis of the experimental data were performed according to the indicators: mean, standard deviation and coefficient of variation (CV). The coefficient of variation is a statistical measure of the dispersion of data and it represents the ratio of the standard deviation to the mean. The smaller the coefficient of variation, the greater the data homogeneity and the smaller the variation. The calculation of the coefficient of variation was important because the relative measurement of variation enables the comparison of different experimental data.

3. Results and Discussion

3.1. Microstructural Characterization of Inconel 718

For microstructural analysis, the two types of specimens (as-fabricated and heat-treated) were cut from the bottom of the sandwich structures. The polished samples were etched with aqua regia (70% HCl + 30% HNO_3) to reveal the microstructure. The typical microstructure [14,15,44–47] of the as-fabricated sample sliced in vertical cross section—parallel to the building direction and perpendicular to the building direction—at low magnification observed with optical microscope is shown in (Figure 4a), respectively (Figure 4b).

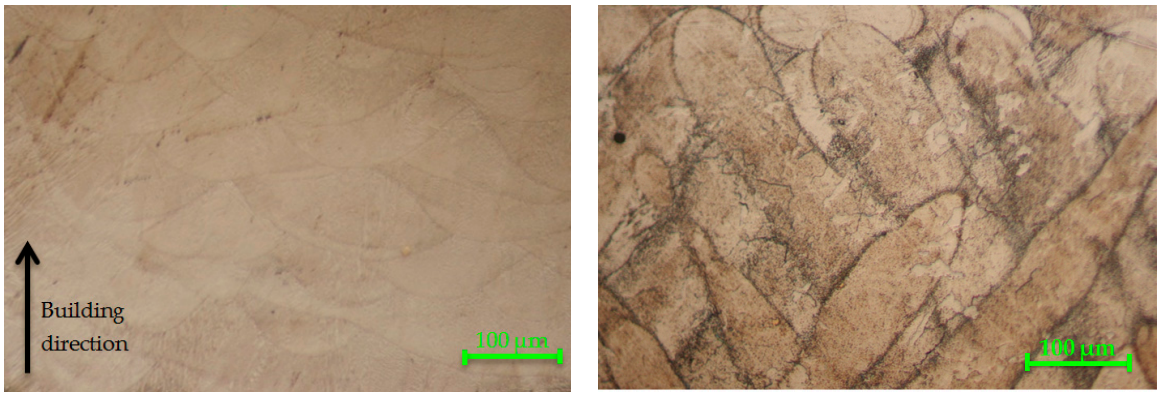

(**a**) (**b**)

Figure 4. *Cont.*

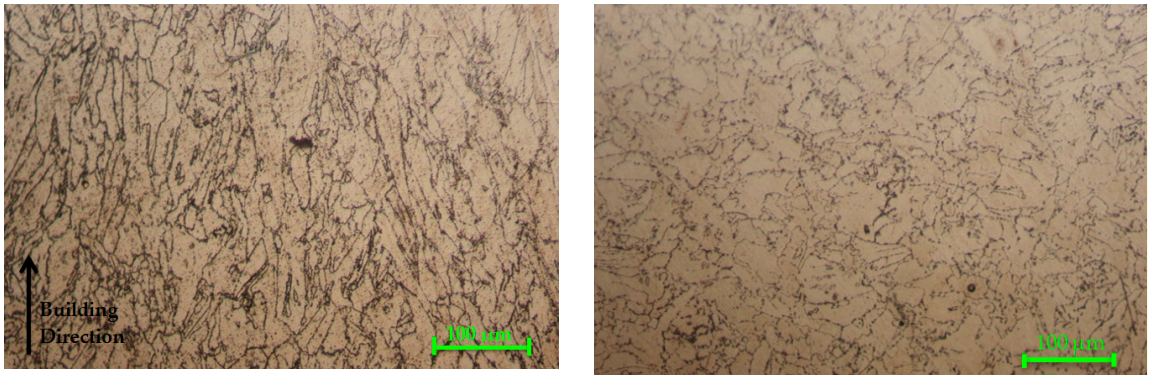

(**c**) (**d**)

Figure 4. Optical micrographs of SLMed Inconel 718 samples: (**a**) vertical cross section (magnification 200×) of as-fabricated samples; (**b**) Perpendicular plane to the building direction (magnification 200×) of as-fabricated samples; (**c**) Vertical cross section (magnification 200×) of heat treatment samples; (**d**) Perpendicular plane to the building direction (magnification 200×) of heat treatment samples.

The typical microstructural [8,14,44–46] of the samples after the homogenization heat treatment and the microstructure of the as-fabricated samples along vertical cross section (parallel to the building plane) are shown in Figure 4c and respectively along the perpendicular plane to the building direction (parallel to the scanning plane) are shown in Figure 4d. The as-fabricated microstructure of the Inconel 718 samples viewed in the building plane (Figure 4a) depicts the columnar grain structure within the melting pools. The microstructure of Inconel 718 after homogenization significantly differs from microstructure of the sample before homogenization heat treatment. Nevertheless, after homogenization heat treatment process, the optical microstructure image of Inconel 718 illustrates the relatively homogeneous and irregular fine grain structure (Figure 4c,d). It was evident that the heat homogenization treatment (solution treatment + double aging) of Inconel 718 samples have the significant effect on the whole microstructural proprieties increased. After homogenization heat treatment, there were no directed columnar cells or traces of laser path present in Figure 4c,d, characteristics which can be seen on specimens after SLM (Figure 4a,b). The microstructure of the specimens changed significantly after the homogenization heat treatment was conducted, in both reference planes (vertical cross section plane and respectively along the perpendicular plane to the building direction) so that the cellular dendritic structures and columnar grain structures can no longer be observed and instead of the melting pool boundaries, the grains and grain boundaries have appeared. However, even at this homogenization temperature, the melting pool boundaries have not completely disappeared. In addition, after the homogenization treatment of the specimens elongated grains have appeared with different size and fine-dispersed uniformly distributed precipitates mainly gathered in the grain boundary areas.

3.2. Compressive Behavior of Sandwich Structures

For the compression tests 4 sets of 5 samples each were used, as follows: 5 as-fabricated sandwich structures with perforated skin (acronym As-fabricated SSPS); 5 as-fabricated sandwich structures with perforated core (acronym As-fabricated SSPC); 5 heat-treated sandwich structures with perforated skin (acronym heat-treated SSPS); 5 heat-treated sandwich structures with perforated core (acronym heat-treated SSPC).

Twenty samples of the sandwich structure were tested under compression (Figure 5a), until the appearance of fracture. With the help of the corresponding universal testing machine WDW-150S software was determined the load–displacement curves and the mechanical characteristics (compressive strength and compressive modulus) of the analyzed Inconel 718 sandwich structures.

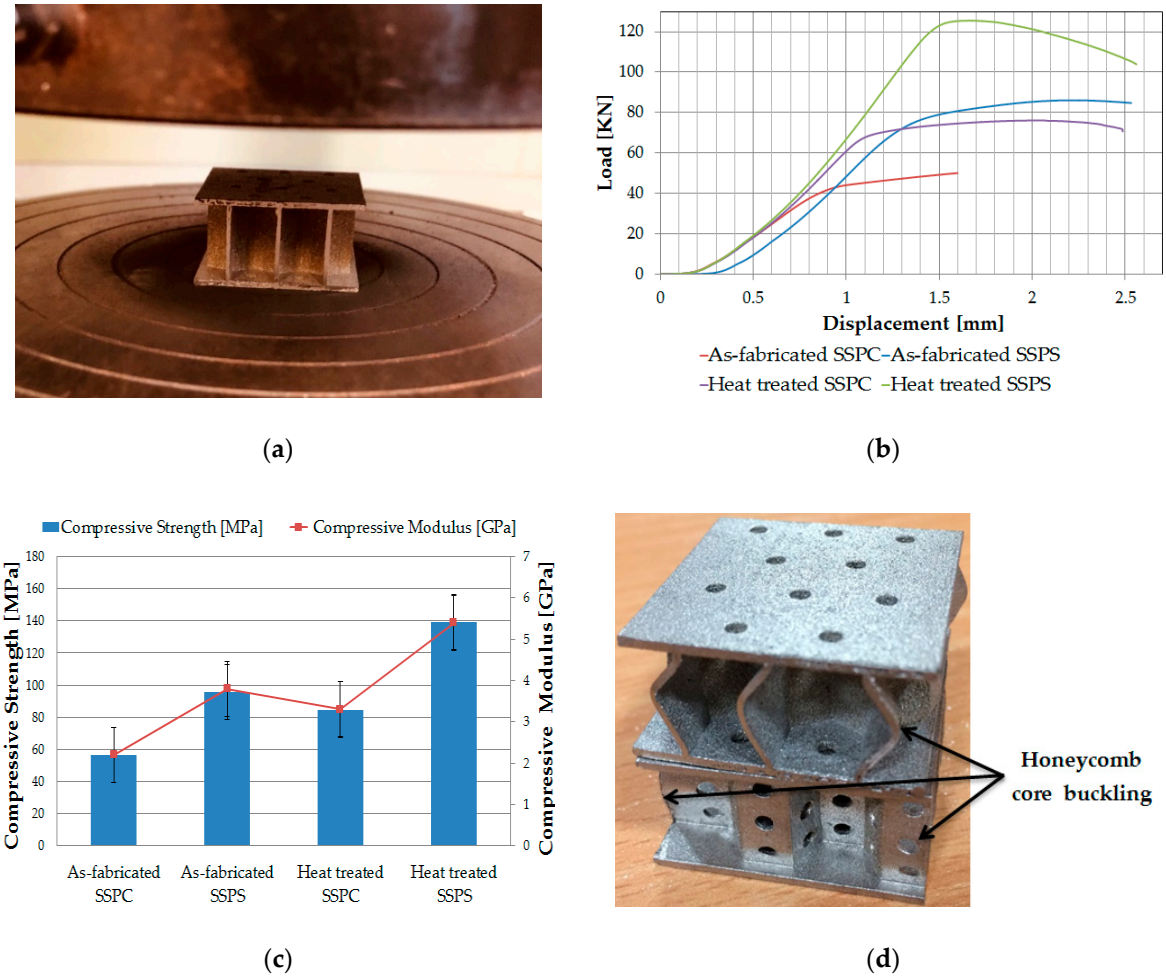

Figure 5. Compression test of SLMed Inconel 718 sandwich structures: (**a**) flatwise compression testing of as-fabricated SSPS; (**b**) load–displacement compression curves of the Inconel 718 sandwich structures; (**c**) compressive strength and compressive modulus of the Inconel 718 sandwich structures; (**d**) buckling of honeycomb cores of the Inconel 718 sandwich structures.

The compression characteristic curve of load–displacement was created by averaging the values that resulted from of the testing of 5 samples. This curve is shown in graphic form in Figure 5b.

The behavior, in terms of load–displacement of the twenty samples in static compression shows a linear relationship between the applied force and the displacement increase and then a decrease in the maximum force at the time of damage of the Inconel 718 sandwich structures. When testing the as-fabricated SSPS, the platen of the test machine was close to the specimen, but without being in contact with it. Thus, there was a distance at which the machine recorded only displacement without loading the specimen. In conclusion, this gap of load–displacement curve of as-fabricated SSPS (Figure 5b) does not affect the compression test result at all.

For the Inconel 718 sandwich structures, the program of the compression testing machine allowed for the calculation of mechanical characteristics, such as compressive strength and compressive modulus. As shown in Figure 5c, the compressive strength varied between 56.65 MPa (as-fabricated SSPC) and 139.4 MPa (heat-treated SSPS), and the compressive modulus stayed within the values of 2.2 GPa and 5.4 GPa.

In several studies the compression testing of sandwich structures was analyzed for various skins materials as well as for the core structure. Hu et al. [48] performed compression tests on the bio-inspired sandwich structures manufactured by SLM technology, made from Ti6Al4 V material and obtained a compressive strength of approximately 200 MPa. In addition, Shifa et al. [49] determined

the compressive performance of sandwich structures with aluminum honeycomb core and reinforced epoxy composite facing, and the values for the compressive strength were 4.26 MPa. A recent study conducted by Li et al. [50] shows that the compressive strength for different thicknesses of the honeycomb core (5–15 mm) varies between 0.8 MPa and 2.2 MPa. Sandwich structures with a hierarchical square honeycomb core and glass fiber/epoxy composite face sheets have a compressive strength of 15 MPa [51]. Overall, the honeycomb core sandwich structures manufactured and tested in this study have a higher compressive strength than those made from composite and metal materials. In contrast, sandwich structures made from Ti6Al4 V metal powder by SLM have a higher compressive strength (200 MPa) compared to sandwich structures made from Inconel 718 metal powder, which were compression tested in this study.

The coefficient of variation represents an important numerical characteristic that offers data about the dispersal associated with a random variable, relative to the mean value. A low value of the variation coefficient reflects a low degree of uncertainty of the random variable, whereas a high value of the variation coefficient determines a high degree of uncertainty. In the case studies from the engineering field, usually the value of the coefficient of variation has to be between 1% and 30% [52]. For the Inconel 718 sandwich structures tested at compression, the main statistical indicators were determined (Tables 2 and 3). Corresponding to the data presented in Tables 2 and 3, the uncertainty of the four sets of experimental data (compressive strength and compressive modulus) was relatively low and shows the values CV = 4.72% (for compressive strength) and CV = 6.82% (for compressive modulus).

Table 2. Statistical indicators determined through the static compression tests results of the Inconel 718 sandwich structures—compressive strength (MPa).

Sample Type	Mean (MPa)	Standard Deviation (MPa)	Coefficient of Variation (CV)%
As-fabricated SSPC	56.65	1.77	3.14
As-fabricated SSPS	95.6	2.91	3.05
Heat-treated SSPC	84.8	4	4.72
Heat-treated SSPS	139.4	3.7	2.66

Table 3. Statistical indicators determined through the static compression tests results of the Inconel 718 sandwich structures—compressive modulus (MPa).

Sample Type	Mean (GPa)	Standard Deviation (GPa)	Coefficient of Variation (CV)%
As-fabricated SSPC	2.2	0.15	6.82
As-fabricated SSPS	3.8	0.22	5.79
Heat-treated SSPC	3.3	0.1	3.03
Heat-treated SSPS	5.4	0.31	5.74

If the variation coefficient is close to zero (CV < 30%), then the statistical studied data (for compressive strengths and compressive modules) were homogenous and the mean was representative for each sets of values. Analyzing the as-fabricated sandwich structures it can be concluded that the SSPS shows superior performance compared to the SSPC.

In addition, from Figure 5c it is observed that the heat-treated SSPS showed the best performances in compression tests having compression strength and a higher compression modulus than the heat-treated SSPC.

The mean values of the compressive strengths from as-fabricated and heat-treated occurs in similar proportions (for both structures), because the manufacturing process using the SLM technology and the homogenization heat treatment presented the same parameters and the same conditions. Thus, the compressive strengths for the two structures (SSPS and SSPC), after the homogenization heat treatment, showed an increase of approximately 50%.

The compressive strength of SSPS specimens was superior to that of SSPC specimens because the core structure plays the most important role in compression tests, being assimilated to the main structures that take over most of the load. By comparison, the skin of the sandwich structure was a secondary structure, which takes over the load and transmits it to the core. Thus, the compressive strength was normally higher in the case of the core without holes compared to the perforated core. The introduction of holes in the core of the sandwich structure causes stress concentrators and areas with high buckling deformation.

All compression-tested sandwich structures had the same deformation mechanism, namely, the buckling of the honeycomb core (Figure 5d). Thus, the sandwich structures suffered a crushing of the honeycomb core, while the skin showed no failures.

In this study, the sandwich structures were designed in order to be able to observe the compression behavior of both structures, namely the: full honeycomb core and the open honeycomb core. Following the compression tests, the same deformation mode was observed in both structures, namely: the local buckling of the core. In addition, a greater deformation of the open honeycomb core can be observed, due to the redistribution of the load on the honeycomb core, especially in the corner or open cell areas.

3.3. Microhardness Test

Of the mechanical properties, the microhardness testing of the samples manufactured by SLM technology represents an intensely researched field. In numerous studies [1,19,53–55], a negligible difference for microhardness in planes parallel and perpendicular to the building direction was reported of AM Inconel 718 samples. While some studies have shown negligible microhardness variation [55,56], the others have mentioned that the microhardness decreases through the build height [25,57] of AM Inconel 718 samples fabricated by SLM technology.

For the Vickers microhardness testing four samples were collected from the sandwich structures, manufactured by SLM in order to determine their microhardness characteristics. Microhardness tests were performed on vertical cross section (parallel to the building direction) of the as-fabricated and heat-treated samples. The samples were cut from the top and from the bottom of sandwich structures to analyze the variation of microhardness on the build height.

The test results indicated that there was an obvious change of microhardness on vertical cross section plane surface for Inconel 718 alloys fabricated by SLM on bottom and from the top section, as for the as-fabricated samples as well as for heat-treated samples. In the as-fabricated condition, the mean microhardness value on bottom section was 369.59 $HV_{0.1}$ with an increase of 13% compared to the top section. For the heat-treated sample, the mean microhardness value on bottom section was 521.15 $HV_{0.1}$ with an increase of 14% compared to the top section.

The mean microhardness value of the homogenization heat-treated Inconel 718 sample was measured, so on the bottom section was 521.15 $HV_{0.1}$ and, respectively on the top section was 456.01 $HV_{0.1}$. Thereby it was confirmed that even in the case of heat-treated specimens, the microhardness decreases through the build height. It can also be observed that the microhardness of the heat-treated specimens increased by 40% for the samples analyzed in the upper section and by 41% for the samples analyzed in the lower section, compared to as-fabricated samples.

The higher microhardness at the bottom of the sandwich structure was attributed to enhanced precipitation hardening due to the repetitive heating cycles experienced by the bottom region of the sandwich structure during the SLM process. The bottom of the sandwich structure was subjected to a repetitive heating cycle, which was assimilated to a heat treatment which results in a higher microhardness. The lower value of microhardness at the top of the sandwich structure may be due to a decrease of the strengthening phase. At the top of the sandwich structure, the laser only travels over the surface once and there were no subsequent heat treatments and similar findings on microhardness changes were reported in other studies [1,45,53].

The results obtained in this study regarding the microhardness tests, that were also investigated in other studies [1,22,24] confirm that the microhardness shows a percentage increase between 20% and

50% following the heat treatment, compared to the untreated samples of Inconel 718 alloy, manufactured by SLM technology. The superior compressive strength and microhardness of heat-treated AM Inconel 718 specimens compared to as-fabricated specimens were mainly attributed to the precipitation hardening process resulting from the homogenization heat treatment, as mentioned in previous studies [9,13,44].

In the field of engineering, the practical use of the coefficient of variation sets the threshold for switching from a homogeneous data set (the percentage was between 0–30%) to heterogeneous data (more than 30%). The values of the coefficient of variation (Table 4) for the microhardness results were between 1.319–5.138%, which determines homogeneity of the experimental data and the mean value was representative for the microhardness values.

Table 4. Statistical indicators of microhardness of the Inconel 718 sample.

Sample Type	Mean ($HV_{0.1}$)	Standard Deviation ($HV_{0.1}$)	Coefficient of Variation (CV)%
As-fabricated sample—top section	324.9	4.287	1.319
As fabricated sample—bottom section	369.59	9.066	2.453
Heat-treated sample—top section	456.01	12.685	2.781
Heat-treated sample—bottom section	521.15	26.778	5.138

3.4. Finite Element Analyses of the Inconel 718 Sandwich Structures

Finite element simulation of the Inconel 718 sandwich structures was performed in the statics module of the ANSYS Workbench 19 R3. In the simulation model, the dimension of the Inconel 718 sandwich structures, the material properties of the samples (Inconel 718), top platen and bottom platen were set up in agreement with that of compression tests. The sandwich structures model was established by SolidWorks 2019 software and then was imported into the Ansys Workbench software to generate mesh. The elastic–plastic model was used for the skin sandwich structure and honeycomb core in the finite element analysis. The contacts between the top platen and the sandwich structure were set as a frictionless support. Between the bottom platen and sandwich structure were set as a fixed support (Figure 6a). Friction was considered between the top platen and the upper skin of the sandwich structures and the frictional coefficient was 0.15. The value of the coefficient of friction for the contact between the top platen and the sandwich structure was chosen to be 0.15 because the flat-compression test platen were made of hardened steel and the faces of the platen were cleaned with oil to minimize the friction. Skins were assumed to be perfectly bonded with honeycombs cores. In addition, the displacement rate of the top platen was 2 mm/min and the bottom platen was fixed. Figure 6b shows the finite element mesh of the Inconel 718 honeycomb sandwich structures. The bottom and top platen were discretized using hexahedral elements with 20 nodes and the mesh size was 2 mm. Tetrahedral elements with 10 nodes with mesh size of 0.5 mm were used in the entire mesh for the honeycomb core and the skins of the Inconel 718 sandwich structures.

Finite element analysis of the Inconel 718 honeycomb sandwich structures was conducted with the following results being obtained: comparative analysis of the deformation behavior of the compression tested specimens with that of the finite element analysis of the same specimens; comparative analysis of the distribution of stresses resulting from experimental tests and FEA simulations; comparative analysis of the maximum reaction forces that appeared in the compression tests and the reaction forces that appeared in the lower platen for the FEA model. The comparative analysis was performed for: the as-fabricated sandwich structures with perforated skin (as-fabricated SSPS) and for the as-fabricated sandwich structures with perforated core (as-fabricated SSPC).

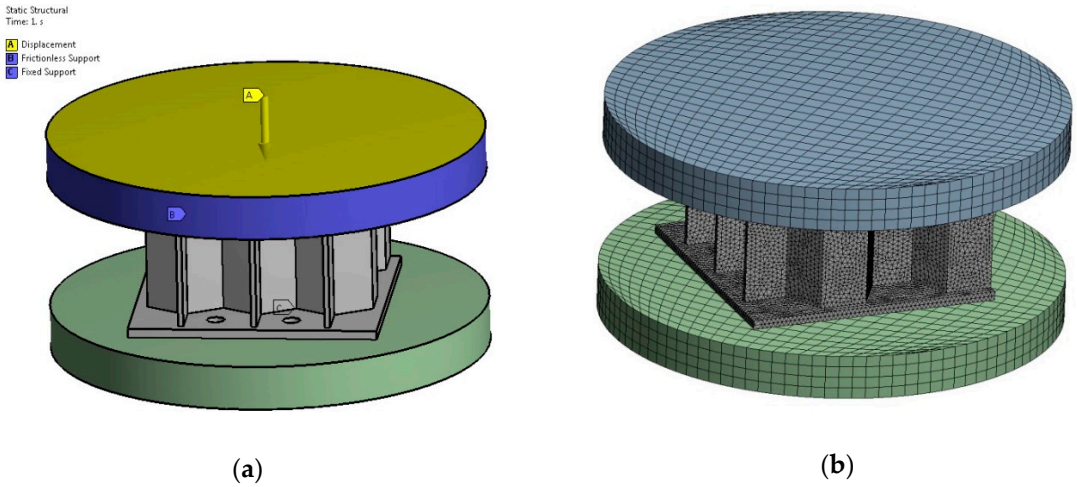

(**a**) (**b**)

Figure 6. Finite element analysis of the honeycomb sandwich samples: (**a**) finite-element mesh model; (**b**) boundary conditions of Inconel 718 honeycomb sandwich structures.

Hence, after examining the specimens subjected to compression tests and those analyzed with finite elements it can be stated that the deformation mode appears, in both cases, at the core of the structure (Figure 7a,b). Thus, it can be observed that the core of the two sandwich structures, analyzed with FEA, shows the same deformation mode as that of the compression tested specimens, namely the buckling of the honeycomb core. The total deformation presents the maximum value at a middle section of the sandwich structures.

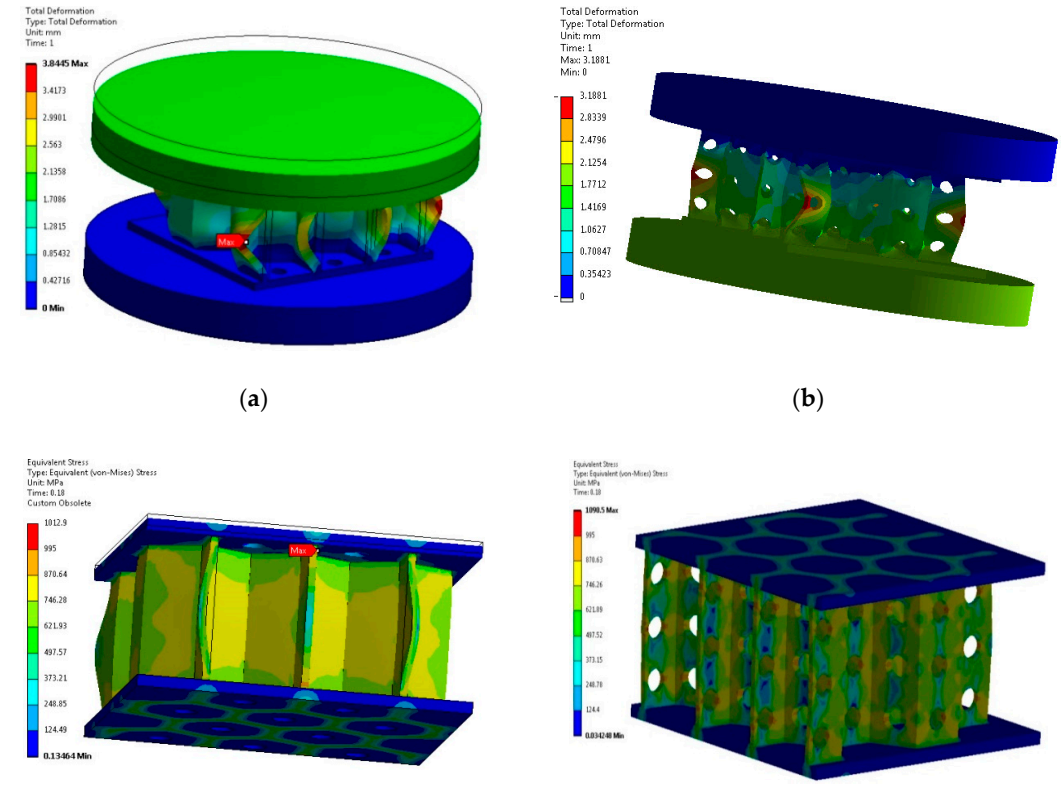

(**c**) (**d**)

Figure 7. FEA results of Inconel 718 honeycomb sandwich structures: (**a**) field of total deformations of as-fabricated SSPS; (**b**) field of total deformations of as-fabricated SSPC; (**c**) field of equivalent von Mises stress of as-fabricated SSPS; (**d**) field of equivalent von Mises stress of as-fabricated SSPC.

The failure mechanism of the sandwich structure was closely related to its equivalent stress distribution, so it was necessary to analyze the stress of the sandwich structure in the case of compressive tests. The as-fabricated sandwich structures with perforated skin (Figure 7c) showed the maximum value of the equivalent stress at the joint between the core and the skin, as this structure has good core rigidity. In contrast, the maximum equivalent stress for the as-fabricated sandwich structures with perforated core has a maximum value in the honeycomb core hole area. The maximum equivalent stress in this case (Figure 7d) was due to the stress concentration which appears in the area of the perforated holes of the honeycomb core.

The reaction forces of the sandwich structure were studied using the commercial finite element analysis software, ANSYS Workbench 19 R3. The result of the comparative study, between the reaction forces resulting from the experimental tests (compression) and the reaction forces that appeared in the lower plate from the finite element analysis (Table 5), presents an adequate validation of the information measured and used in the testing of the specimens and of the FEA model, the errors that appear between these results were within 2.71% and 3.32%. The finite elements models provided good results and the reaction forces calculated with FEA simulation was very close to that forces obtained with the compression tests.

Table 5. Error analysis of reaction forces between experimental tests and FEA simulations.

Sample Type	Reaction Forces—Compression Tests (KN)	Reaction Forces—FEA Simulations (KN)	Relative Error (%)
As-fabricated SSPS	86.06	83.2	3.32
As-fabricated SSPC	50.06	48.7	2.71

Figure 8. compares the load–displacement curves for the results of experimental analyzes and FEA simulations for as-fabricated specimens subjected to three-point bending. It can be seen that there was a good agreement between the load–displacement curves obtained from the experimental tests and those obtained from the FEA simulation of the sandwich specimens. In conclusion, it can be stated that the FEA model shows similar results, both in terms of the value of the reaction forces and the shape of the load–displacement curves, compared to the compression tests of the sandwich specimens.

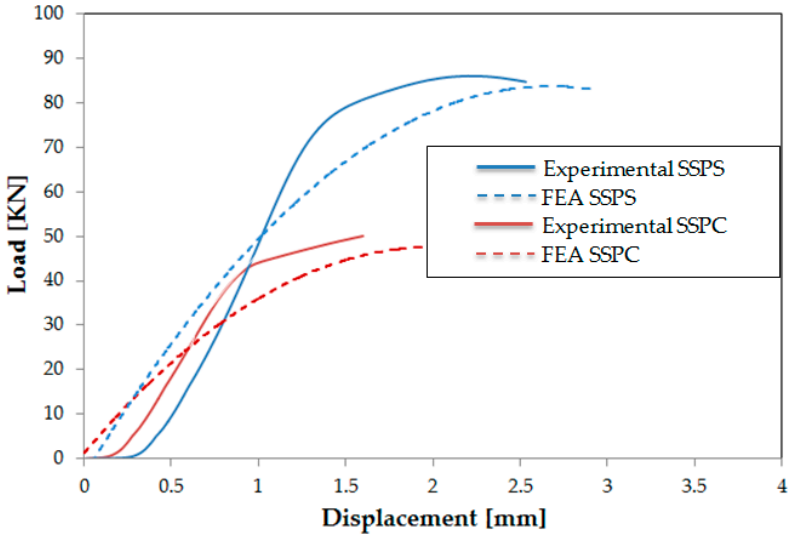

Figure 8. Comparison of experiment and simulation FEA—load–displacement curves.

4. Conclusions

In this study, honeycomb core sandwich structures with two different topologies were manufactured for the first time directly by laser selective melting technology. The two topologies

were designed and manufactured taking into account the constraints on the selective laser melting technology. Thus, in order to be able to extract the metallic powders from the inside of the honeycomb cell, the core or skin were provided with holes. The two types of sandwich structures with perforated core or skin were manufactured directly by SLM technology and then subjected to a homogenization heat treatment.

The as-fabricated samples and heat-treated samples were observed by light microscopy and microhardness tests on these samples were performed. In the microscopic analyses, the Inconel 718 specimens showed a typical structure of the parts manufactured by the SLM technology. The microscopic images were analyzed before and after the homogenization heat treatment, cut after a section on the vertical cross section and perpendicular to the building direction.

In addition, after the compression tests the following results were obtained: as-fabricated sandwich structures with perforated skin showed a compressive strength 69% higher compared to as-fabricated sandwich structures with perforated core; heat-treated sandwich structures with perforated skin have a compressive strength 65% higher than heat-treated sandwich structures with perforated core; after the homogenization heat treatment, the two topologies of sandwich structures showed an increase of about 50% of the compressive strength.

The microhardness tests were investigated on vertical cross section of the as-fabricated and heat-treated samples. Following the microhardness tests the next conclusions were obtained: the microhardness decreases through the build height; the microhardness of the heat-treated specimens increased by approximately 40% in both the upper and lower sections, compared to the non-heat-treated specimens.

The comparison analysis between the results of compression tests and finite elements analysis indicated that there was a good agreement between those which implies that the FEA simulation can be used instead of time-consuming experimental procedures to study the effect of different parameters on the mechanical performances of the Inconel 718 honeycomb sandwich structures. The results were in good agreement with the experimental results and showed the maximum relative error of only 3.32% between the reaction forces experimentally and from the FEA simulations. In this study, the feasibility of direct manufacture of honeycomb core sandwich structures using SLM technology was demonstrated.

Author Contributions: Conceptualization, S.M.Z.; methodology S.M.Z., M.A.P., L.A.C., C.L.; software, C.L., experimental investigation, M.A.P., S.M.Z., L.A.C.; resources, S.M.Z.; data curation, S.M.Z., C.L.; writing—original draft preparation, S.M.Z., M.A.P., L.A.C., C.L.; writing—review and editing, S.M.Z., M.A.P., L.A.C., C.L.; visualization, S.M.Z., M.A.P.; supervision, S.M.Z.; project administration, S.M.Z.; funding acquisition, S.M.Z. All authors have read and agreed to the published version of the manuscript.

Funding: This work was supported by a mobility grant of the Romanian Ministry of Research and Innovation, CNCS-UEFISCDI, project number PN-III-P1-1.1-MC-2017-0418, within PNCDI III.

Acknowledgments: This work was supported by a mobility grant of the Romanian Ministry of Research and Innovation, CNCS-UEFISCDI, project number PN-III-P1-1.1-MC-2017-0418, within PNCDI III. We hereby acknowledge the structural funds project PRO-DD (POS-CCE, O.2.2.1, ID 123, SMIS 2637, ctr. No 11/2009) for providing the infrastructure used in this work.

Conflicts of Interest: The authors declare no conflict of interest.

References

1. Hosseini, E.; Popovich, V.A. A review of mechanical properties of additively manufactured Inconel 718. *Addit. Manuf.* **2019**, *30*, 100877. [CrossRef]
2. Wang, X.; Chou, K. Microstructure simulations of Inconel 718 during selective laser melting using a phase field model. *Int. J. Adv. Manuf. Technol.* **2019**, *100*, 2147–2162. [CrossRef]
3. Pollock, T.M.; Tin, S. Nickel-Based Superalloys for Advanced Turbine Engines: Chemistry, Microstructure, and Properties. *J. Propuls. Power* **2006**, *22*, 361–374. [CrossRef]

4. Popovich, V.A.; Borisov, E.V.; Popovich, A.A.; Sufiiarov, V.S.; Masaylo, D.V.; Alzina, L. Functionally graded Inconel 718 processed by additive manufacturing: Crystallographic texture, anisotropy of microstructure and mechanical properties. *Mater. Des.* **2017**, *114*, 441–449. [CrossRef]
5. Popovich, V.A.; Borisov, E.V.; Popovich, A.A.; Sufiiarov, V.S.; Masaylo, D.V.; Alzina, L. Impact of heat treatment on mechanical behaviour of Inconel 718 processed with tailored microstructure by selective laser melting. *Mater. Des.* **2017**, *131*, 12–22. [CrossRef]
6. Li, X.; Shi, J.J.; Cao, G.H.; Russell, A.M.; Zhou, Z.J.; Li, C.P.; Chen, G.F. Improved plasticity of Inconel 718 superalloy fabricated by selective laser melting through a novel heat treatment process. *Mater. Des.* **2019**, *180*, 107915–107922. [CrossRef]
7. Liu, P.; Hu, J.; Sun, S.; Feng, K.; Zhang, Y.; Cao, M. Microstructural evolution and phase transformation of Inconel 718 alloys fabricated by selective laser melting under different heat treatment. *J. Manuf. Process.* **2019**, *39*, 226–232. [CrossRef]
8. Feng, K.; Liu, P.; Li, H.; Sun, S.; Xu, S.; Li, J. Microstructure and phase transformation on the surface of Inconel 718 alloys fabricated by SLM under 1050 °C solid solution + double ageing. *Vacuum* **2017**, *145*, 112–115. [CrossRef]
9. Chlebus, E.; Gruber, K.; Ku, B.; Kurzac, J.; Kurzynowski, T. Effect of heat treatment on the microstructure and mechanical properties of Inconel 718 processed by selective laser melting. *Mater. Sci. Eng. A* **2015**, *639*, 647–655. [CrossRef]
10. Mostafa, A.; Rubio, I.P.; Brailovski, V.; Jahazi, M.; Medraj, M. Structure, texture and phases in 3D printed IN718 alloy subjected to homogenization and HIP treatments. *Metals* **2017**, *7*, 196. [CrossRef]
11. Cherry, J.A.; Davies, H.M.; Mehmood, S.; Lavery, N.P.; Brown, S.G.R.; Sienz, J. Investigation into the effect of process parameters on microstructural and physical properties of 316L stainless steel parts by selective laser melting. *Int. J. Adv. Manuf. Technol.* **2015**, *76*, 869–879. [CrossRef]
12. Luo, S.; Huang, W.; Yang, H.; Yang, J.; Wang, Z.; Zeng, X. Microstructural evolution and corrosion behaviors of Inconel 718 alloy produced by selective laser melting following different heat treatments. *Addit. Manuf.* **2019**, *30*, 100875. [CrossRef]
13. Raghavan, S.; Zhang, B.; Wang, P.; Sun, C.N.; Nai, M.L.S.; Li, T.; Wei, J. Effect of different heat treatments on the microstructure and mechanical properties in selective laser melted INCONEL 718 alloy. *Mater. Manuf. Proc.* **2017**, *32*, 1588–1595. [CrossRef]
14. Yao, X.; Moon, S.K.; Lee, B.Y.; Bi, G. Effects of heat treatment on microstructures and tensile properties of IN718/TiC nanocomposite fabricated by selective laser melting. *Int. J. Precis. Eng. Manuf.* **2017**, *18*, 1693–1701. [CrossRef]
15. Zhang, D.; Feng, Z.; Wang, C.; Wang, W.; Liu, Z.; Niu, W. Comparison of microstructures and mechanical properties of Inconel 718 alloy processed by selective laser melting and casting. *Mater. Sci. Eng. A* **2018**, *724*, 357–367. [CrossRef]
16. Zhao, J.-R.; Hung, F.-Y.; Lui, T.-S. Erosion Resistance and Particle Erosion-Induced Tensile Embrittlement of 3D-Selective Laser Melting Inconel 718 Superalloy. *Metals* **2020**, *10*, 21. [CrossRef]
17. Yi, J.; Kang, J.; Wang, T.; Wang, X.; Hu, Y.; Feng, T.; Feng, Y.; Wu, P. Effect of laser energy density on the microstructure, mechanical properties, and deformation of Inconel 718 samples fabricated by selective laser melting. *J. Alloys Compd.* **2019**, *786*, 481–488. [CrossRef]
18. Nguyen, Q.B.; Luu, D.N.; Nai, S.M.L.; Zhu, Z.; Chen, Z.; Wei, J. The role of powder layer thickness on the quality of SLM printed parts. *Arch. Civ. Mech. Eng.* **2018**, *18*, 948–955. [CrossRef]
19. Konecna, R.; Kunz, L.; Nicoletto, G.; Baca, A. Long fatigue crack growth in Inconel 718 produced by selective laser melting. *Int. J. Fatigue* **2016**, *92*, 499–506. [CrossRef]
20. Moussaoui, K.; Rubio, W.; Mousseigne, M.; Sultan, T.; Rezai, F. Effects of selective laser melting additive manufacturing parameters of Inconel 718 on porosity, microstructure and mechanical properties. *Mater. Sci. Eng. A* **2018**, *735*, 182–190. [CrossRef]
21. Jia, Q.; Gu, D. Selective laser melting additive manufacturing of Inconel 718 superalloy parts: Densification, microstructure and properties. *J. Alloys Compd.* **2014**, *585*, 713–721. [CrossRef]
22. Tucho, W.M.; Cuvillier, P.; Sjolyst-Kverneland, A.; Hanson, V. Microstructure and hardness studies of Inconel 718 manufactured by selective laser melting before and after solution heat treatment. *Mater. Sci. Eng. A* **2017**, *689*, 220–232. [CrossRef]

23. Lu, Y.J.; Wu, S.Q.; Gan, Y.L.; Huang, T.T.; Yang, C.G.; Junjie, L.; Lin, J.X. Structure on the microstructure, mechanical property and residual stress of SLM Inconel-718 alloy manufactured by differing island scanning strategy. *Opt. Laser Technol.* **2015**, *75*, 197–206. [CrossRef]
24. Wang, Z.; Guan, K.; Gao, M.; Li, X.; Chen, X.; Zeng, X. The microstructure and mechanical properties of deposited-IN718 by selective laser melting. *J. Alloys Compd.* **2012**, *513*, 518–523. [CrossRef]
25. Wang, X.; Keya, T.; Chou, K. Build Height Effect on the Inconel 718 Parts Fabricated by Selective Laser Melting. *Proced. Manuf.* **2016**, *5*, 1006–1017. [CrossRef]
26. Amato, K.N.; Gaytan, S.M.; Murr, L.E.; Martinez, E.; Shindo, P.W. Microstructures and mechanical behavior of Inconel 718 fabricated by selective laser melting. *Acta Mater.* **2012**, *60*, 2229–2239. [CrossRef]
27. Luo, Z.; Zhao, Y. Efficient thermal finite element modeling of selective laser melting of Inconel 718. *Comput. Mech.* **2020**, *65*, 763–787. [CrossRef]
28. Andreotta, R.; Ladani, L.; Brindley, W. Finite element simulation of laser additive melting and solidification of Inconel 718 with experimentally tested thermal properties. *Finite Elem. Anal. Des.* **2017**, *135*, 36–43. [CrossRef]
29. Mukherjee, T.; Zhang, W.; DebRoy, T. An improved prediction of residual stresses and distortion in additive manufacturing. *Comput. Mater. Sci.* **2017**, *126*, 360–372. [CrossRef]
30. Romano, J.; Ladani, L.; Sadowski, M. Laser additive melting and solidification of Inconel 718: Finite element simulation and experiment. *Jom* **2016**, *68*, 967–977. [CrossRef]
31. Tsai, S.-N.; Taylor, A.C. Vibration behaviours of single/multi-debonded curved composite sandwich structures. *Compos. Struct.* **2019**, *226*, 111291. [CrossRef]
32. Zaharia, S.M.; Lancea, C.; Chicos, L.A.; Pop, M.A.; Caputo, G.; Serra, E. Mechanical properties and corrosion behaviour of 316l stainless steel honeycomb cellular cores manufactured by selective laser melting. *Trans. FAMENA* **2017**, *41*, 11–24. [CrossRef]
33. Lam, Q.; Patil, D.; Le, T.; Eppley, T.; Salti, Z.; Goss, D.; Grishin, A.; Bhate, D. An examination of the low strain rate sensitivity of additively manufactured polymer, composite and metallic honeycomb structures. *Materials* **2019**, *12*, 3455. [CrossRef] [PubMed]
34. McGregor, D.J.; Tawfick, S.; King, W.P. Mechanical properties of hexagonal lattice structures fabricated using continuous liquid interface production additive manufacturing. *Addit. Manuf.* **2019**, *25*, 10–18. [CrossRef]
35. Maconachie, T.; Leary, M.; Lozanovski, B.; Zhang, X.; Qian, M.; Faruque, O.; Brandt, M. SLM lattice structures: Properties, performance, applications and challenges. *Mater. Des.* **2019**, *183*, 1–18. [CrossRef]
36. Kotzem, D.; Arold, T.; Niendorf, T.; Walther, F. Damage Tolerance Evaluation of E-PBF-Manufactured Inconel 718 Strut Geometries by Advanced Characterization Techniques. *Materials* **2020**, *13*, 247. [CrossRef]
37. Hazeli, K.; Babamiri, B.B.; Indeck, J.; Minor, A.; Askari, H. Microstructure-topology relationship effects on the quasi-static and dynamic behavior of additively manufactured lattice structures. *Mater. Des.* **2019**, *176*, 107826. [CrossRef]
38. Babamiri, B.B.; Askari, H.; Hazeli, K. Deformation mechanisms and post-yielding behavior of additively manufactured lattice structures. *Mater. Des.* **2020**, *188*, 108443. [CrossRef]
39. Selective Laser Melting Machine SLM®280 2.0. Available online: https://www.slm-solutions.com/fileadmin/user_upload/121EN180808-02-002-SLM280-20_WEB3.pdf (accessed on 1 March 2020).
40. Material Data Sheet Ni-Alloy IN718 / 2.4668-SLM Solutions. Available online: https://www.slm-solutions.com/fileadmin/user_upload/MDS_Ni-Alloy_IN718_2.4668_0219.pdf (accessed on 1 March 2020).
41. Metal Powder Inconel 718-Optimized for Selective Laser Melting. Available online: https://www.slm-solutions.com/fileadmin/user_upload/Metal_Powder_1912_02_Web.pdf (accessed on 1 March 2020).
42. Rao, G.A.; Kumar, M.; Srinivas, M.; Sarma, D.S. Effect of standard heat treatment on the microstructure and mechanical properties of hot isostatically pressed superalloy inconel 718. *Mater. Sci. Eng. A* **2003**, *A355*, 114–125. [CrossRef]
43. SAE Aerospace. *Aerospace Material Specification, AMS 5662*; SAE International: Warrendale, PA, USA, 2009.
44. Karabulut, Y.; Tascioglu, E.; Kaynak, Y. Heat treatment temperature-induced microstructure, microhardness and wear resistance of Inconel 718 produced by selective laser melting additive manufacturing. *Optik* **2019**, 163907. [CrossRef]
45. Tian, C.; Li, X.; Liu, Z.; Zhi, G.; Guo, G.; Wang, L.; Rong, Y. Study on grindability of Inconel 718 superalloy fabricated by selective laser melting (SLM). *Stroj. Vestn. J. Mech. Eng.* **2018**, *64*, 319–328.

46. Popovich, A.A.; Sufiiarov, V.S.; Polozov, I.A.; Borisov, E.V. Microstructure and mechanical properties of Inconel 718 produced by SLM and subsequent heat treatment. *Key Eng. Mater.* **2015**, *651*, 665–670. [CrossRef]
47. Popovich, V.A.; Borisov, E.V.; Heurtebise, V.; Riemslag, T.; Popovich, A.A.; Sufiiarov, V.S. Creep and thermomechanical fatigue of functionally graded Inconel 718 produced by additive manufacturing. In *TMS 2018 147th Annual Meeting & Exhibition Supplemental Proceedings*; Springer: Berlin/Heidelberg, Germany, 2018; pp. 85–97.
48. Hu, K.; Lin, K.; Gu, D.; Yang, J.; Wang, H.; Yuan, L. Mechanical properties and deformation behavior under compressive loading of selective laser melting processed bio-inspired sandwich structures. *Mater. Sci. Eng. A* **2019**, *762*, 138089. [CrossRef]
49. Shifa, M.; Tariq, F.; Baloch, R.A. Effect of Carbon Nanotubes on mechanical properties of honeycomb sandwich panels. *Nucleus* **2017**, *54*, 1–6.
50. Li, Z.; Ma, J. Experimental Study on Mechanical Properties of the sandwich composite structure reinforced by basalt fiber and nomex honeycomb. *Materials* **2020**, *13*, 1870. [CrossRef] [PubMed]
51. Côté, F.; Russell, B.P.; Deshpande, V.S.; Fleck, N.A. The through-thickness compressive strength of a composite sandwich panel with a hierarchical square honeycomb sandwich core. *J. Appl. Mech.* **2009**, *76*, 061004. [CrossRef]
52. Zaharia, S.M.; Morariu, C.O.; Nedelcu, A.; Pop, M.A. Experimental study of static and fatigue behavior of CFRP-balsa sandwiches under three-point flexural loading. *BioResources* **2017**, *12*, 2673–2689. [CrossRef]
53. Stevens, E.L.; Toman, J.; To, A.C.; Chmielus, M. Variation of hardness, microstructure and laves phase distribution in direct laser deposited alloy 718 cuboids. *Mater. Des.* **2017**, *119*, 188–198. [CrossRef]
54. Gribbin, S.; Bicknell, J.; Jorgensen, L.; Tsukrov, I.; Knezevic, M. Low cycle fatigue behavior of direct metal laser sintered Inconel alloy 718. *Int. J. Fatigue* **2016**, *93*, 156–167. [CrossRef]
55. Strondl, A.; Palm, M.; Gnauk, J.; Frommeyer, G. Microstructure and mechanical properties of nickel based superalloy IN718 produced by rapid prototyping with electron beam melting (EBM). *Mater. Sci. Technol.* **2011**, *27*, 876–883. [CrossRef]
56. Zhang, Q.L.; Yao, J.H.; Mazumder, J. Laser direct metal deposition technology and microstructure and composition segregation of Inconel 718 superalloy. *J. Iron Steel Res. Int.* **2011**, *18*, 73–78. [CrossRef]
57. Tian, Y.; McAllister, D.; Colijn, H.; Mills, M.; Farson, D.; Nordin, M.; Babu, S. Rationalization of microstructure heterogeneity in Inconel 718 builds made by the direct laser additive manufacturing process. *Metall. Mater. Trans. A* **2014**, *45*, 4470–4483. [CrossRef]